

Relative stability of $6H$ -SiC{0001} surface terminations and formation of graphene overlayers by Si evaporation

Jochen Rohrer,^{1,*} Eleni Ziambaras,² and Per Hyldgaard¹

¹*BioNano Systems Laboratory, Department of Microtechnology, MC2, Chalmers University of Technology, SE-412 96 Gothenburg*

²*Materials and Surface Theory Group, Department of Applied Physics, Chalmers University of Technology, SE-412 96 Gothenburg*

(Dated: July 24, 2021)

We present density functional theory (DFT) calculations for $6H$ -SiC{0001} surfaces with different surface stackings and terminations. We compare the relative stability of different (0001) and (000 $\bar{1}$) surfaces in terms of their surface free energies. Removing surface and subsurface Si atoms, we simulate the formation of graphene and graphene-like overlayers by Si evaporation. We find that overlayers with a different nature of bonding are preferred at the two non-equivalent surface orientations. At (0001), a chemically bonded, highly strained and buckled film is predicted. At (000 $\bar{1}$), a van der Waals (vdW) bonded overlayer is preferred. We quantify the vdW binding and show that it can have a doping effect on electron behavior in the overlayer.

PACS numbers: 68.65.Pq,73.22.Pr,73.20.At

I. INTRODUCTION

Graphene [1] is a highly interesting material for future nanoelectronic devices [2, 3] such as transistors [4], integrated circuits [5] or detectors [6]. This is because of its unique electronic properties but also, and more importantly, because of the possibility to adjust and control these properties. The nature and magnitude of conduction and overall (opto-) electronic properties can be modified, for example, by applying electric fields [7], by adsorbants [8, 9], by utilizing finite-size effects [10, 11] or by an environment-induced material transformation into graphane [12, 13] or graphane oxide [14].

An important issue for the use of graphene and graphene-derivatives [15] for devices is the actual influence of substrates (on which these materials are placed in the device) on the bandstructure and hence on electron behavior. Although graphene and its derivatives do not tend to easily form chemical bonds to other materials, van der Waals (vdW) interactions will always be present. For the fully hydrogenated graphene-derivative, graphane [12, 13], we [16] have recently reported first-principles vdW density functional (vdW-DF) calculations [17], predicting that vdW interactions stabilize multilayer formation. Moreover, we predict that the electron behavior in the graphane multilayer may deviate, at least locally, from the behavior in the monolayer [16]. Similar effects must naturally also be expected when graphene is simply exposed to a substrate. Indeed, combinations of vdW-DF and GW [18] calculations for graphene on various metal surfaces have already predicted that the vdW interaction can shift the graphene Fermi level [19] and that these shifts can be either positive or negative, depending on the the actual substrate material.

In this paper, we study graphene and graphene-like overlayers at $6H$ -SiC{0001} surfaces, focusing on vdW binding and the effect of vdW forces on electron behavior. The $6H$ -SiC{0001} surfaces are a natural choice for studying general substrate-graphene vdW interactions. SiC is regarded as promising substrate candidate for large-scale fabrication of pure graphene by Si evaporation from {0001} surfaces [20–22]. We first characterize the thermodynamic stability of SiC{0001} surfaces with different orientations, atomic stacking and surface termination. We then simulate the Si evaporation by removing Si atoms from surface and subsurface layers, letting the systems find their new ground state. At (0001), we predict a chemically bonded, strongly buckled and stretched graphene-like overlayer. At (000 $\bar{1}$), we predict a flat vdW-bonded graphene overlayer. For the vdW-bonded overlayer we perform band-structure calculations and find a modified electron behavior indirectly induced through vdW forces.

The paper is organized as follows. In Sec. II, we give a short background of SiC and its {0001} surfaces. We present details of our computational method in Sec. III. In Sec. IV we present our results for the stability of various surfaces and surface/overlayer systems, vdW binding between SiC and graphene and the resulting band structure. The results are discussed in Sec. V and we summarize and conclude our work in Sec. VI.

II. MATERIALS BACKGROUND

A. Bulk SiC

Figure 1 details the atomic structure of $6H$ -SiC. The crystal structure is hexagonal. Table I presents a comparison of the lattice parameters obtained from experiment [23] and from our first-principle calculations described further below.

*Electronic address: rohrer@chalmers.se

Along the c -axis, the bulk repeat unit is composed of six SiC bilayers. Each bilayer contains 50 % silicon and 50 % carbon and forms a buckled honeycomb lattice. We define the $[0001]$ direction as indicated in the figure. With this definition, the Si atoms in each bilayer are located above (along $[0001]$) the center-of-mass plane, C atoms are located below.

The stacking sequence (along $[001]$) is $ABC A' C' B'$. We use primes to distinguish the first A , B , and C layers in each repeat unit from the second ones. Because of the six layers in the repeat unit, naively one would expect twelve possible surface terminations for each surface orientation. Due to symmetry, however, each two of the twelve terminations per surface are equivalent. A rotation by 180° around the c axis, maps A sites on A sites, B sites on C sites and C sites on B sites. Therefore, the rotated stacking is $A' C' B' A B C$ showing the equivalence of A and A' sites, B and C' sites, and C and B' sites.

B. Surfaces

Figure 2 shows six out of the twelve different (ideal) $6H$ -SiC $\{0001\}$ surface configurations. Along the $[0001]$ direction, the $6H$ crystal structure lacks inversion symmetry. Thus, the corresponding (0001) surface (the so-called nominally Si-terminated surface [24]) and $(000\bar{1})$ surface (the so-called nominally C-terminated surface [24]) are different. For each surface orientation there are six different possible ideal terminations, corresponding to two chemically different terminations (Si or C) times three structurally different terminations. Ideal here means that we only consider full-coverage surfaces. In practice, a large surface may exhibit partial coverage to counteract a diverging surface dipole [25] and there may be surface reconstructions as to saturate surface dangling bonds.

The top panels show the set of three most natural (flat) Si-terminated (0001) surfaces. These are denoted by Si1, Si2, and Si3. In a Si1 surface, the surface Si atoms are located on top of C atoms that are located in the first subsurface SiC bilayer. In Si2 and Si3 surfaces, the surface Si atoms are correspondingly located on top of C atoms in the second and third subsurface SiC bilayer. The C-terminated counterparts (C1, C2, and C3) are obtained by adding an additional C layer on top of the surface Si layer.

The set of bottom panels displays C-terminated $(000\bar{1})$ surfaces. The three surfaces are denoted by $C\bar{1}$, $C\bar{2}$ and

	exp (Ref. 23)	present
a in Å	3.073	3.091
c in Å	15.118	15.181

TABLE I: Comparison of SiC bulk lattice parameters from experiment and our first-principle calculations.

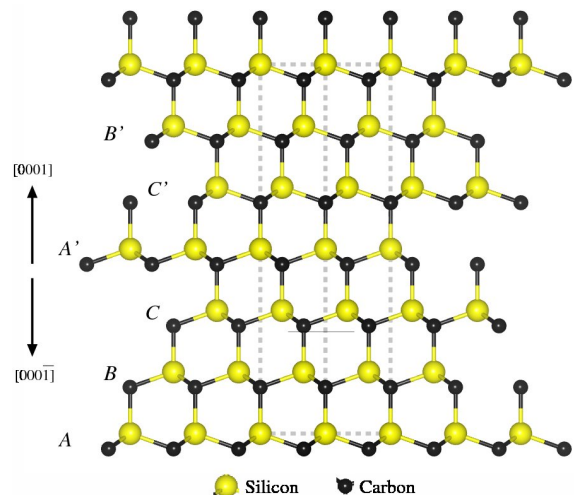


FIG. 1: (Colour online) Bulk structure of $6H$ -SiC. Si atoms are represented by yellow (light gray), large spheres; C atoms are represented by black (black), small spheres. The light gray dashed lines represent the unit cell.

$C\bar{3}$. In a $C\bar{1}$ surface, the surface C atoms are located on top of Si atoms that are located in the first subsurface SiC bilayer. In $C\bar{2}$ and $C\bar{3}$ surfaces, the surface C atoms are correspondingly located on top of Si atoms in the second and third subsurface SiC bilayer. The Si-terminated counterparts (Si $\bar{1}$, Si $\bar{2}$, and Si $\bar{3}$) are obtained by adding an additional Si layer on top of the surface C layer.

At the (0001) surface, C atoms bind only to a single Si atom below; they possess three dangling bonds. Si atoms, on the other hand, bind to three nearest-neighbor C atoms; they only possess one dangling bond. At $(000\bar{1})$, the situation is reversed. Therefore, in the absence of complex reconstructions, the (0001) surface is intuitively expected to be Si terminated (and therefore denoted as the nominally Si-terminated surface [24]) and the $(000\bar{1})$ surface is intuitively expected to be C terminated (and therefore denoted as the nominally C-terminated surface [24]).

III. COMPUTATIONAL METHOD

A. Surface and overlayer stability

All surface and surface/overlayer calculations are performed with the planewave pseudopotential [26] DFT code `dacapo` [27] and the PBE [28] functional for exchange and correlation. We use a planewave cutoff of 400 eV and a $(4 \times 4 \times 1)$ k-point sampling [29] Force relaxations are performed until the residual force is less than 0.03 eV/Å.

We use the supercell approach and represent each surface or surface/overlayer system by slab geometry. The supercells have a height of 40 Å and the lateral dimensions are fixed to accommodate the (1×1) SiC $\{0001\}$

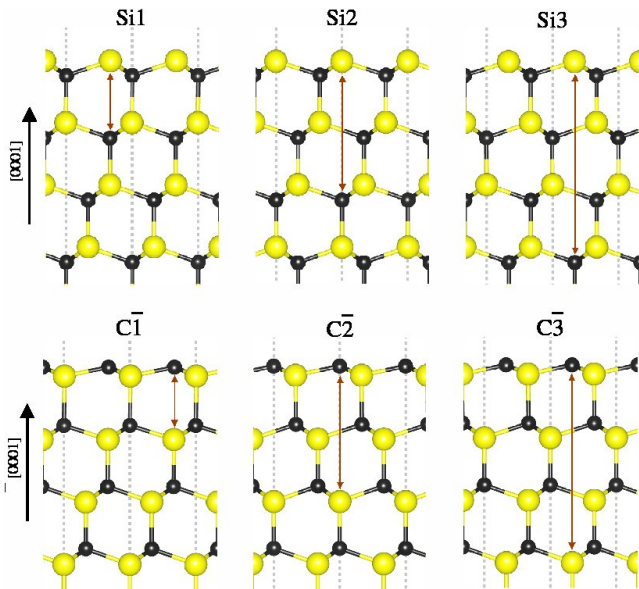


FIG. 2: (Color online) (1×1) $6H$ -SiC(0001) and $(000\bar{1})$ surfaces with different details stacking in the outermost layers. Color coding as in Fig. 1. The set of top panels shows the three nonequivalent (0001) surfaces with Si termination Si1, Si2 and Si3 (see text for a definition of this labeling). Corresponding C-terminated surfaces (C1, C2 and C3) are obtained by adding a C layer on top of terminating Si layer. The set of bottom panels shows the three nonequivalent $(000\bar{1})$ surfaces with C termination $C\bar{1}$, $C\bar{2}$ and $C\bar{3}$. Corresponding Si-terminated surfaces ($Si\bar{1}$, $Si\bar{2}$ and $Si\bar{3}$) are obtained by adding a Si layer on top of the terminating C layer.

surface. Surfaces with different stackings and chemical terminations are represented by slabs of different thicknesses, varying from 9 and 15 bilayers (plus one optional excess Si or C layer). Also, we saturate dangling bonds at the $(000\bar{1})$ [(0001)] side of the slab that represents the (0001) [$(000\bar{1})$] surface by attaching H atoms. Because of the asymmetry of the slabs, we use a dipole correction [30]. With respect to thickness, the calculated surface-energy differences, see Table II, are converged by at least ± 2 meV/ \AA^2 . We have tested this accuracy by comparing surface energies of equivalent surfaces that are represented by slabs of different thicknesses. Specifically, any surface represented by a particular slab can be recovered by addition of three SiC bilayers.

B. Thermodynamic comparison of chemically different terminations

We determine the equilibrium surface preference by comparing surface free energies [31, 32]. Due to the lack of inversion symmetry along $[0001]$, use of slab geometry only enables us to calculate the sum (denoted by $\tilde{\sigma}$ and defined below) of the two surface energies (denoted by σ) corresponding to the (0001) surface and the $(000\bar{1})$ surface. However, keeping the geometry and chemical

composition fixed at one side of the slab, we ensure that the contribution to $\tilde{\sigma}$ from that side is always the same. We thus can compare the relative stability of different structures and compositions at the other side (not fixed) by considering the difference in $\tilde{\sigma}$ for various stackings and terminations.

We define the sum of the two surface free energies as

$$\tilde{\sigma} = \frac{1}{A} \left(E_{\text{slab}} - n_{\text{Si}} \epsilon_{\text{SiC}} - (n_{\text{C}} - n_{\text{Si}}) \mu_{\text{C}} - n_{\text{Gr}} \epsilon_{\text{Gr}} \right). \quad (1)$$

Here, E_{slab} is the total energy of the $6H$ -SiC surface slab, including a possible graphene-like overlayer, that contains n_{Si} silicon atoms (per supercell), n_{C} carbon atoms that belong to the SiC and n_{Gr} carbon atoms that belong to the graphene overlayer. Furthermore, ϵ_{SiC} denotes the energy of one stoichiometric unit of bulk SiC, ϵ_{Gr} is the energy of graphene,¹ and μ_{C} is carbon chemical potential. We note that we have assumed equilibrium between the bulk and the surface, $\epsilon_{\text{SiC}} = \mu_{\text{Si}} + \mu_{\text{C}}$.

The values of the carbon chemical potential in (1) are restricted to a finite range. If the carbon chemical potential is larger than the free energy per carbon atom in graphene ($\mu_{\text{C}} > g_{\text{graphene}}$), the formation of (additional) graphene overlayers becomes more favorable. If, on the other hand, the silicon chemical potential is larger than the free energy per silicon atom in bulk Si (with diamond structure, $\mu_{\text{Si}} > g_{\text{Si}}$), the formation of bulk Si is more favorable. Therefore, the allowed range of the carbon chemical potential is

$$g_{\text{graphene}} \geq \mu_{\text{C}} \geq g_{\text{SiC}} - g_{\text{Si}}. \quad (2)$$

We also introduce

$$\Delta\sigma_{ij} = \tilde{\sigma}_i - \tilde{\sigma}_j, \quad (3)$$

from which we infer the relative stability of surfaces with identical orientations but different stackings and chemical compositions.

C. van der Waals binding

In Sec. IV B, we identify a chemically non-binding SiC(000 $\bar{1}$)/graphene system as thermodynamically stable. We study this system further using the van der Waals density functional (vdW-DF) method [17]. In particular we use the nonlocal correlation functionals $E_{\text{c}}^{\text{nl-1}}$ and $E_{\text{c}}^{\text{nl-2}}$ of Refs. 33 and 34, respectively.

We calculate the energy variation, including vdW forces, by a postprocessing method as follows. We first perform traditional DFT calculations (using the PBE exchange-correlation functional) for various separations

¹ This energy must contain the strain energy since the graphene overlayer is highly expanded in a SiC surface cell.

between the SiC and the graphene overlayer. In these calculations we choose the lateral dimensions of the unit cell to fit those of a (4×4) SiC(000 $\bar{1}$) surface. This allows us to study a (4×4) SiC(000 $\bar{1}$)/ (5×5) graphene system in which the graphene overlayer is hardly strained at all. We use a $(3 \times 3 \times 1)$ k-point sampling to ensure an accurate electronic density for further evaluations of nonlocal correlations according to

$$E^{\text{vdW-DF-}v}[n] = E_0^v[n] + E_c^{\text{nl-}v}[n]. \quad (4)$$

Here, $E_c^{\text{nl-}v}[n]$ is the correlation energy from one of the non-local functionals of Refs. 33 ($v = 1$) and 34 ($v = 2$). Also, in Eq. (4), $E_{0-v}[n]$ is given by

$$E_0^v = E_{\text{tot}}^{\text{PBE}} - E_{\text{xc}}^{\text{PBE}} + E_c^{\text{VWN}} + E_x^v, \quad (5)$$

where E_c^{VWN} is the VWN-LDA [35] correlation energy and $E_x^{v=1} = E_x^{\text{revPBE}}$ and $E_x^{v=2} = E_x^{\text{rPW86}}$ are the revPBE [36] and rPW86 (refitted form of PW86) [37] exchange functionals.

We determine the vdW binding separation and energy by finding the minimum in the layer-binding energy defined as

$$E_{\text{bind}}(d) = E_{\text{vdW-DF}}(d) - E_{\text{vdW-DF}}(d \rightarrow \infty). \quad (6)$$

Here, d is the distance between the surface layer and the overlayer. For a detailed description of a robust implementation of the evaluation of Eq. (6), we refer to Refs. 38–41.

D. Band-structure calculations

We also perform band-structure calculations for (5×5) graphene on (4×4) SiC(000 $\bar{1}$) to probe the effect of vdW bonding on electron behavior. The band-structure calculations are performed as follows. We fix the SiC-graphene separation at the value predicted by the vdW-DF2 calculations and determine the density with a $(4 \times 4 \times 1)$ k-point sampling to ensure a high accuracy in our large unit-cell calculations. This density is subsequently used to perform traditional GGA calculations of the energy spectra at various k points. We focus on the special Brillouin-zone points $\Gamma = (0, 0, 0)$, $K = (2/3, 1/3, 0)$ and $M = (1/2, 1/2, 0)$ and the lines along $\overline{K\Gamma}$, $\overline{\Gamma M}$, and \overline{KM} .

Since we are interested in band-structure modifications, we also perform the same type of calculations for a single graphene layer. In order to not encounter modifications that may be solely due to a (very small) variation in the graphene lattice parameter, we use the same unit cell as in the case for the SiC/graphene system.

IV. RESULTS

A. Relative stability of clean 6H-SiC{0001} surfaces

a. Stacking preference for fixed chemical termination.
Table II compares surface energies for surfaces with

(0001)	$\Delta\sigma$ [meV/Å ²]	(000 $\bar{1}$)	$\Delta\sigma$ [meV/Å ²]
Si1	6.7	Si $\bar{1}$	1.9
Si2	0	Si $\bar{2}$	0
Si3	1.7	Si $\bar{3}$	0.3
C1	4.6	C $\bar{1}$	0
C2	0	C $\bar{2}$	3.0
C3	1.3	C $\bar{3}$	3.5

TABLE II: Differences in surface energies for surfaces with identical orientations and terminations (which makes the numbers independent of the chemical potentials) but with different detailed stacking of the outermost surface layers. The energetically most favorable surface for each orientation and termination is chosen as reference and therefore characterized by $\Delta\sigma = 0$. The effect of surface vibrations is not included.

	$\sigma_{\text{Si}} - \sigma_{\text{C}}$ in meV/Å ² at		
	$\mu_{\text{C}}^{\text{min}}$	$\mu_{\text{C}}^{\text{mid}}$	$\mu_{\text{C}}^{\text{max}}$
1×1 (0001)	-527	-502	-476
$\sqrt{3} \times \sqrt{3}$ (0001)	-559	-534	-509
3×3 (0001)	-539	-513	-487
1×1 (000 $\bar{1}$)	-128	-102	-77
$\sqrt{3} \times \sqrt{3}$ (000 $\bar{1}$)	-75	-49	-23
3×3 (000 $\bar{1}$)	-118	-93	-67

TABLE III: Preference of surface chemical composition at 6H-SiC{0001}. The table lists differences in surface free energies between Si- and C-terminated surfaces for three values of the chemical potential of C. A negative value indicates higher stability of the Si-terminated surface.

identical orientations and identical chemical compositions but with a different detailed stacking of the surface layers. For each orientation and chemical composition of the surface, we choose the configuration with lowest surface energy, or more precisely with lowest $\tilde{\sigma}$, as reference. This configuration is thus characterized by $\Delta\sigma = 0$.

We find that the surface-energy differences are of the order of a few meV/Å². These values are close to or below the actual accuracy of our calculations. Thus, the surface-energy differences between surfaces with different stackings are too small to be of significant importance for determining the stable surface configuration.

b. Chemical composition. In Table III we determine the preferred chemical composition of the (0001) and (000 $\bar{1}$) surfaces. For each orientation we list differences in surface free energies between Si- and C-terminated surfaces at three different values of the C chemical potential. The three values of the C chemical potential correspond to its maximal value, its minimal value, and the value in between.

We find that, within the entire allowed range of the C chemical potential, the Si-terminated surfaces possesses lowest free surface energy, independent of the orientation. For (0001) orientation, this coincides with the expectations on the basis of the number of dangling bonds. For

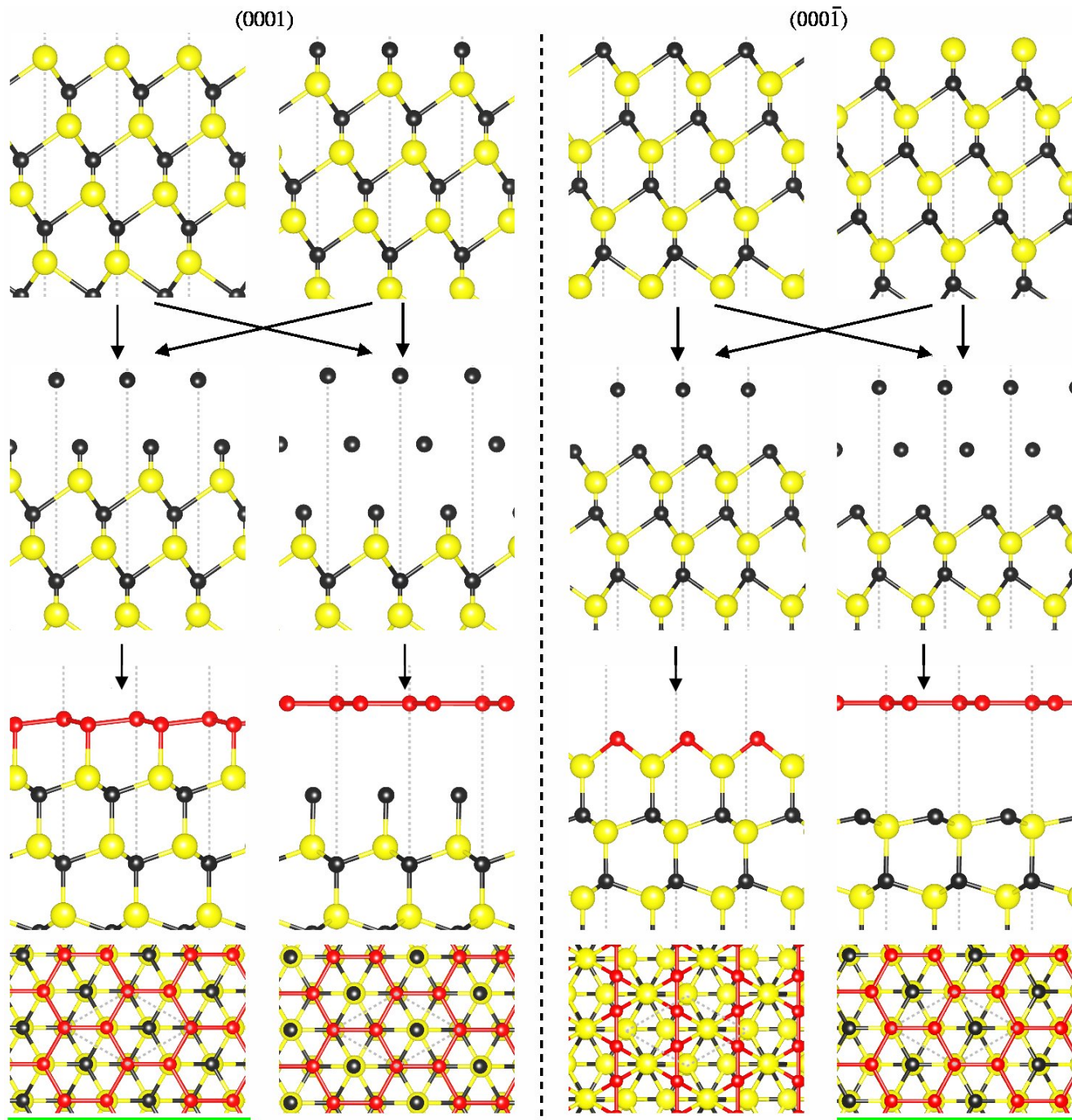


FIG. 3: (Color online) Formation of graphitic overlayers at $\text{SiC}\{0001\}$. Color coding as in Fig. 1; in addition, C atoms forming an overlayer are in red (dark gray) and connected through bonds. The set of top panels shows side views on truncated (0001) and $(000\bar{1})$ surface structures with either Si or C termination. The set of mid-panels shows side views the same structures (*i.e.* unrelaxed), but with (sub) surface Si layers removed. The set of bottom panels shows side and top views on the geometries obtained by relaxing the systems in the mid-panels. At each surface there exist chemically bonded systems (first and third column in the bottom set of panels) and systems that are not chemically bonded (second and fourth set of panels). Our thermodynamics analysis indicates that the chemically bonded system is the stable one at $\text{SiC}(0001)$; At $\text{SiC}(000\bar{1})$, the chemically non-binding configuration is stabilized. The stable, that is, thermodynamically favored configurations are underlined in green (gray).

(000 $\bar{1}$) surfaces, the predictions appear counterintuitive. There, the Si-terminated surface possesses more dangling bonds than the C-terminated surface and should therefore be less favorable.

Table III also reports that the perhaps counterintuitive result for (000 $\bar{1}$) surfaces remains unaltered when considering larger surface unit-cells that allow for surface reconstructions (without considering more complex surface terminations than pure Si or C termination, however), such as ($\sqrt{3} \times \sqrt{3}$) and (3×3) surface unit-cells. Details of our calculations concerning surface reconstructions are documented in the supplementary material.

The apparent equilibrium preference of Si-terminated (000 $\bar{1}$) surfaces reflects the rich phase diagram of SiC. Our comparison, limited to full Si and C coverages, is likely not exhaustive enough to capture this richness in a more quantitative manner. On the other hand, resolving the difficult structure is not relevant for our search for carbon overlayers at SiC{0001} surfaces that may form by evaporation of Si atoms.

B. Graphitic overlayer formation by Si evaporation

We now turn our focus towards structure, stability and bonding of graphitic overlayers at SiC{0001}. Figure 3 illustrates the formation of different graphitic overlayers at SiC{0001} surfaces by evaporation of Si atoms [20–22]. We use (1×1) surface unit-cells to study the effect of removing full surface and subsurface layers. As illustrated in the preceding subsection and the supplementary material, the initial surface morphologies can, in principle, be much more complicated. However, since the surface atoms evaporate in a heating process, we expect that the detailed surface structure before heating is of minor importance.

a. Structure. The set of top panels of Fig. 3 shows four (1×1) surfaces with different orientations and terminations. In the set of mid-panels, we have removed surface and subsurface Si atoms. The set of bottom panels presents the geometries that are obtained by relaxing the structures in the set of mid-panels above. The figure also illustrates that the role of the surface composition (and structure) effectively reduces to determining the amount of Si that needs to be evaporated to generate a specific final SiC/graphene system.

At both surface orientations we obtain two types of overlayers. The first type of overlayer is chemically bonded, see first and third column in the set of bottom panels in Fig. 3. As a result the overlayer adopts the SiC lattice parameter resulting in a considerable stretching of the C bonds. At (0001), the overlayer preserves the hexagonal graphene-like shape but also exhibits a buckling. At (000 $\bar{1}$), the hexagonal shape is not preserved. The C atoms arrange themselves in chains located in bridge positions at the surface.

The second type of overlayer is not chemically bonded, see second and fourth column in the set of bottom panels

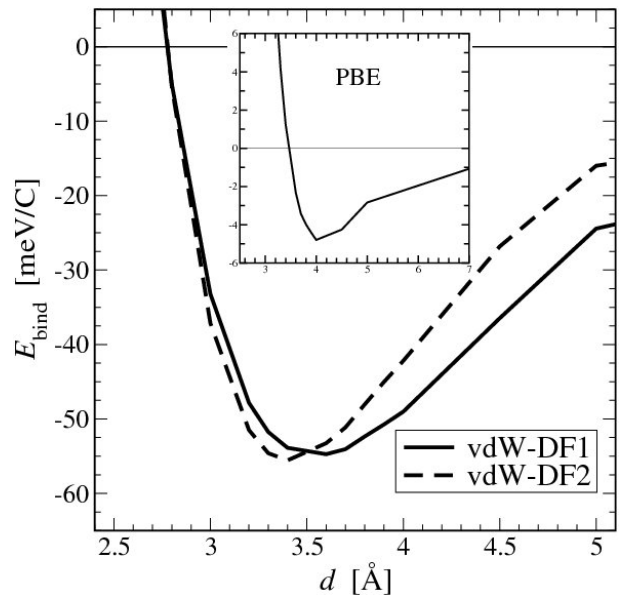


FIG. 4: Energy variation of graphene on SiC(000 $\bar{1}$) including vdW forces.

of Fig. 3. The non-binding character is reflected by the large separations between the overlayers and the outermost surface layers. In both cases, the absence of chemical bonding leaves the ideal hexagonal graphene shape unchanged. We expect that these carbon overlayers contract and adopt the unstrained graphene lattice.

b. Stability. We compare the stability of the different surface/overlayer systems with identical orientations by means of their surface energy, see Eq. (1). For the chemically bonded systems, we consider the overlayer to be in equilibrium with the SiC surface, that is, the number of graphene units is set to zero. For the other two systems, we assume that the chemical potential of the overlayer is not related to that of SiC, but to that of (strained) graphene (so correcting for the strain energy due to the lattice misfit).

At the (0001) surface, we find that the chemically bonded system is more preferred. The surface-energy differences are $86 \text{ meV}/\text{\AA}^2$ at the minimal value of carbon chemical potential and $137 \text{ meV}/\text{\AA}^2$ at the maximal value of carbon chemical potential. At the (000 $\bar{1}$) surface, the chemically non-bonding system is preferred. The corresponding surface-energy differences are $445 \text{ meV}/\text{\AA}^2$ (at μ_C^{min}) and $393 \text{ meV}/\text{\AA}^2$ (at μ_C^{min}).

C. vdW bonded (5×5) graphene at (4×4) SiC(000 $\bar{1}$)

We quantify the vdW binding of graphene at SiC(000 $\bar{1}$) by studying the vdW energy variation of the system shown in the rightmost bottom panel of Fig. 3. In the depicted (1×1) system, the graphene overlayer is highly strained. We therefore use a (4×4) SiC(000 $\bar{1}$) surface unit-cell in our calculations combined with a (5×5)

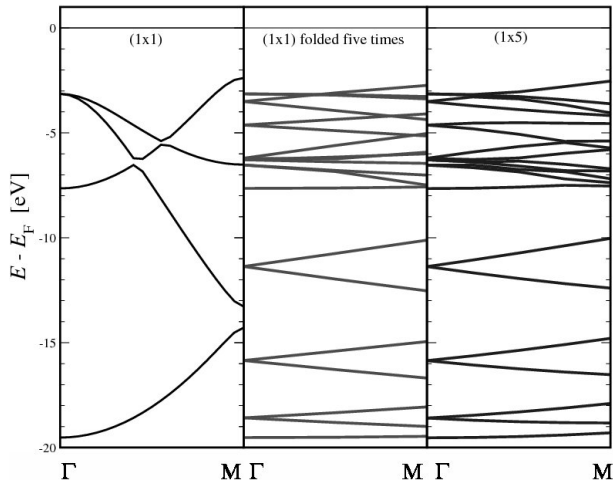


FIG. 5: Zone folding of the graphene band diagram along $\overline{\Gamma M}$. The left panel shows the unfolded calculated (1×1) band structure of graphene. The diagram in the mid-panel is constructed from that in the left by folding five times. The right panel shows the calculated band diagram using a (1×5) graphene unit cell.

graphene overlayer [42] to ensure that the overlayer is almost unstrained (the C-C bond length is stretched by $\sim 0.5\%$ only).

Figure 4 shows the energy variation as a function of the separation between the SiC surface-layer and the graphene overlayer. Both, results using vdW-DF1 and vdW-DF2 are shown. The insert shows that traditional GGA calculations (PBE) do not predict any meaningful binding (notice the different scale on the y -axis in the insert).

The vdW-DF energy variations agree qualitatively. vdW-DF2 predicts a slightly smaller binding separation and a slightly larger binding energy. The numerical values are $d_{\text{bind}} = 3.6 \text{ \AA}$ and $E_{\text{bind}} = -54.7 \text{ meV}$ per carbon atom (in graphene) for vdW-DF1 and $d_{\text{bind}} = 3.4 \text{ \AA}$ and $E_{\text{bind}} = -55.6 \text{ meV}$ per carbon atom for vdW-DF2.

We note that accounting for vdW binding for the chemically non-binding graphene overlayer at SiC(0001) (second panel from the left in bottommost set of panels in Fig. 3) is expected to lower surface energy by a similar amount. However, our calculated values correspond to $\Delta_{\text{vdW}\sigma} \sim 13 \text{ meV/\AA}$. Therefore, even with an account of vdW interactions, the chemisorbed carbon overlayer will still be more preferable than the chemically nonbinding (vdW-bonded) overlayer.

D. Band structure of vdW-bonded graphene at nominally C-terminated SiC(000 $\bar{1}$)

a. Consistency check for zone folding. In Fig. 5 we check that our large unit-cell calculations capture and reliably reproduce the details of the electron behavior, that is, the band-structure physics. The left panel shows

the band structure of graphene (without substrate) along a straight line from Γ to K as calculated within a (1×1) unit cell. In the mid-panel we show a band diagram that is constructed from the left panel by zone folding it five times. The right panel shows the band diagram as

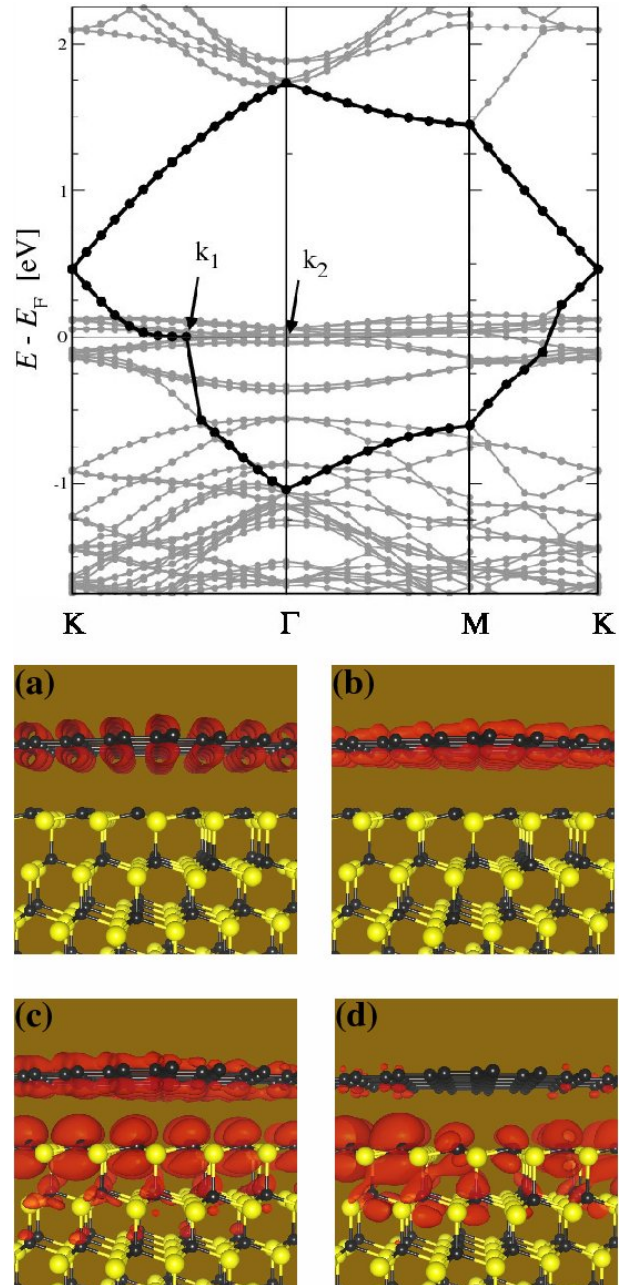


FIG. 6: (Color online) Electronic structure of vdW bonded (5×5) graphene at (4×4) SiC(000 $\bar{1}$). The top panel shows the calculated band diagram along $\overline{K\Gamma}$, $\overline{\Gamma M}$ and \overline{MK} . The UVB and LCB corresponding to graphene are highlighted. The set of bottom panels shows (absolute values of) various wave functions. (a) Graphene UVB WF in K, (b) graphene LCB WF in K, (c) WF in k_1 (see top panel) and (d) WF in k_2 (see top panel).

calculated within a (1×5) unit cell.

The constructed and the calculated zone-folded band diagram agree reasonably well. The slight differences may be due to differences in the underlying electronic densities that are used in the respective calculations and which is transferred from the (1×1) band diagram to the zone-folded diagram.

b. Overlayer band-structure. The top panel of Fig. 6 shows the calculated band diagram of (5×5) graphene at (4×4) SiC(000 $\bar{1}$). We restrict the plot to relevant energy window around the Fermi level. The complex band structure is due to the (5×5) zone folding of graphene bands and the (4×4) zone folding of SiC bands.

Among the many bands, two bands are highlighted. These bands correspond to the upper valence band (UVB) and to the lower conduction band (LCB) in an isolated graphene sheet. We have explicitly checked that the wave functions (WF) corresponding to the UVB and LCB are localized on the graphene overlayer.

The set of bottom panels of Fig. 6 shows various WFs. These WFs are representative for the different types of WF localization in the system. Panels (a) and (b) show that the UVB and LCB WFs in K, for example, are entirely located on the overlayer. WFs fully localized on graphene are typical for the LCB.

We note that a kink arises in the band structure variation as the graphene band crosses the Fermi level at k_1 (see top panel of Fig. 6 for a definition of k_1). There we find that the graphene UVB WF can also be shared between the SiC and the graphene.

Finally, in panel (d), we illustrate that the graphene overlayer also slightly affects the nature of the SiC states at the Fermi level in k_2 (see top panel of Fig. 6 for a definition of k_2). Although most WFs corresponding to a band between the UVB and LCB are fully localized within the SiC substrate, at k_d and other k points, some WFs do have a small weight also on the graphene overlayer.

V. DISCUSSION

A. Surface stability

Our calculations of (1×1) SiC{0001}, including some $(\sqrt{3} \times \sqrt{3})$ and (3×3) reconstructions in the supplementary material, predict a preference for Si termination. This prediction is reasonable for the (0001) surface but surprising for the (000 $\bar{1}$) surface for which we would expect a C termination.

Resolving this discrepancy requires a more careful study that take into account the actual growth conditions of SiC [43] and/or improves on the description of surface reconstructions. The latter task would have to consider a richer set of surface terminations also including excess and deficiency Si or C. However, the size of the $(\sqrt{3} \times \sqrt{3})$ and (3×3) surface unit-cells makes a full

reconstruction-search a large project of its own, requiring systematic structure-search strategies such as considering a larger pool of candidate geometries with structural motifs [44] of the reconstructed surfaces obtained here, evolutionary-type of iteration [45] or other global structure-search methods [46–48].

Such a search for surface reconstructions is clearly beyond the scope of the present work, in particular, since the exact morphology of the stable SiC{0001} surfaces is only of minor importance for the main objective of this paper: the study of modification of electron behavior in graphene overlayers due to vdW interactions. At the same time, we emphasize that our calculated surface energies are upper limits of the true surface energies.

B. Nature of binding in SiC/graphene systems

We have identified preferred SiC/graphene systems as they may result by Si evaporation from various SiC{0001} surfaces. Our results indicate that the nature of binding at the nominally Si-terminated (0001) surfaces is different from the nature of binding at the nominally C-terminated (000 $\bar{1}$) surface.

At (0001), we have identified a chemisorbed, strongly buckled graphene overlayer. At (000 $\bar{1}$), the overlayer is stabilized by vdW forces. The different nature of binding at the two surfaces may have consequences for the quality of graphene that is grown by evaporation of Si from different SiC{0001} faces (at the nominally C-terminated or at the nominally Si-terminated face).

C. Electron behavior in vdW-bonded graphene

Our band-structure calculations for SiC/graphene, see Fig. 6, show that vdW binding can cause a doping-like effect. In free-standing graphene, the density of states (DOS) vanishes at the Fermi level.² On SiC, the vdW binding renders graphene a p-doped metal. The Fermi level is shifted to lower energies into the original valence band where the DOS is finite. The prediction of a Fermi-level shift is similar to the results reported for graphene on various metal surfaces in Ref. 19.

In the present case, vdW binding leads to a further modification in the band-structure. At the new Fermi level between K and Γ , we also observe a kink in the band structure. To the left of k_1 (see Fig. 6) the dispersion in the LCB can be fitted to a parabolic form $E(k) = E_0 + a \cdot (k - k_1)^2$, from which we infer an effective electron

² We have checked that this remains true also if we slightly stretch the C-C bond length such that a (5×5) unit cell is commensurate with a (4×4) SiC{0001} cell.

mass

$$m_{\text{eff}} = \hbar^2 \left[\frac{d^2 E}{dk^2} \right]^{-1}. \quad (7)$$

$m_{\text{eff}} \sim 1.02 \times 10^{-30}$ kg or $m_{\text{eff}} \sim 1.1m_e$ where m_e is the (actual) electron mass.

VI. SUMMARY AND CONCLUSIONS

We present DFT calculations for SiC{0001} surfaces and graphitic overlayers at SiC{0001} surfaces. In particular, we focus on surface and surface/overlayer stability, and on binding and band-structure modifications (due to the binding) of the overlayers.

For surfaces, we study the relative stability as function of the detailed stacking, as function of the chemical composition and to some extent (see supplementary material), as function of the type of reconstruction. We find that the surface-energy differences due to different detailed stacking of the outermost surfaces are below the accuracy of our calculations and not of any significance. For ideally truncated surfaces (no excess or deficiency of Si or C) we find that Si-terminated surfaces are generally more favorable than C-terminated surfaces.

For SiC/overlayer systems we find two different types of overlayers. At SiC(0001), we predict an overlayer that is chemically bonded to the substrate. Because of the chemical bonding this overlayer is expected to significantly differ in its electronic nature from single-layer graphene. At SiC(000 $\bar{1}$), we predict a vdW-bonded overlayer.

In line with Ref. 19, our band-structure calculations for the vdW-bonded graphene show that vdW interactions with a substrate can have a doping effect (here: p doping). As a novel feature, we also identify a kink in the electron dispersion at the Fermi level and calculate an effective mass of $m_{\text{eff}} \sim 1.1m_e$ at the minimum of the conduction band at this kink.

Acknowledgments

We thank T. S. Rahman and S. Hong for valuable discussions. Support by the Swedish National Graduate School in Materials Science (NFSM), the Swedish Research Council (VR), the Swedish Governmental Agency for Innovation Systems (VINNOVA), and the Swedish National Infrastructure for Computing (SNIC) is gratefully acknowledged.

-
- [1] K. S. Novoselov, A. K. Geim, S. V. Morozov, D. Jiang, Y. Zhang, S. V. Dubonos, I. V. Grigorieva, and A. A. Firsov, *Science* **306**, 666 (2004).
- [2] A. K. Geim and K. S. Novoselov, *Nature Materials* **6**, 183 (2007).
- [3] A. K. Geim, *Science* **324**, 1530 (2009).
- [4] L. A. Ponomarenko et al. (2008), *Science* **320**, 356 (2008).
- [5] F. Traversi, V. Russo and R. Sordan, *Appl. Phys. Lett.* **94**, 223312 (2009).
- [6] F. Schedin et al. *Nature Mater* **6**, 652 (2007).
- [7] E. V. Castro, K. S. Novoselov, S. V. Morozov, N. M. R. Peres, J. M. B. Lopes dos Santos, Johan Nilsson, F. Guinea, A. K. Geim, and A. H. Castro Neto, *Phys. Rev. Lett.* **99**, 216802 (2007).
- [8] Z. F. Wang, Q. Li, H. Zheng, H. Ren, H. Su, Q. W. Shi and Jie Chen, *Phys. Rev. B* **75**, 113406 (2007).
- [9] M. Klintonberg, S. Lebegue, M. I. Katsnelson, and O. Eriksson, *Phys. Rev. B* **81**, 085433 (2010).
- [10] V. Barone, A. Hod and G. E. Scuseria, *Nano Lett.* **6**, 2748 (2006).
- [11] M. Y. Han, B. Özyilmaz, Y. Zhang, and P. Kim, *Phys. Rev. Lett.* **98**, 206805 (2007).
- [12] J. O. Sofo, A. S. Chaudhari and G. D. Barber, *Phys. Rev. B* **75**, 153401 (2007).
- [13] D. C. Elias, R. R. Nair, T. M. G. Mohiuddin, S. V. Morozov, P. Blake, M. P. Halsall, A. C. Ferrari, D. W. Boukhvalov, M. I. Katsnelson, A. K. Geim, and K. S. Novoselov, *Science* **323**, 5914 (2009).
- [14] D. A. Dikin, S. Stankovich, E. J. Zimney, R. D. Piner, G. H. B. Dommett, G. Evmenenko, S. T. Nguyen and R. S. Ruoff, *Nature* **448**, 457 (2007).
- [15] S. Park and R. S. Ruoff *Nature Nanotechnology* **4**, 217 (2009).
- [16] J. Rohrer and P. Hyldgaard, accepted for publication in *Phys. Rev. B*.
- [17] D.C. Langreth, B.I. Lundqvist, S.D. Chakarova-Käck, V.R. Cooper, M. Dion, P. Hyldgaard, A. Kelkkanen, J. Kleis, Lingzhu Kong, Shen Li, P.G. Moses, E. Murray, A. Puzder, H. Rydberg, E. Schröder, and T. Thonhauser, *J. Phys.: Condensed Matter* **21**, 084203 (2009).
- [18] L. Hedin, *Phys. Rev.* **139**, A796 (1965); F. Aryasetiawan and O. Gunnarsson, *Rep. Prog. Phys.* **61**, 237 (1998).
- [19] M. Vanin, J. J. Mortensen, A. K. Kelkkanen, J. M. Garcia-Lastra, K. S. Thygesen and K. W. Jacobsen, *Phys. Rev. B* **81**, 081408(R) (2010).
- [20] C. Virojanadara, M. Syväjarvi, R. Yakimova, L. I. Johansson, A. A. Zakharov and T. Balasubramanian, *Phys. Rev. B* **78**, 245403 (2008).
- [21] U. Starke and C. Riedl, *J. Phys.: Condens. Matter* **21**, 134016 (2009).
- [22] C. Virojanadara, R. Yakimova, J. Osiecki, M. Syväjarvi, R. I. G. Uhrberg, L. I. Johansson, and A. A. Zakharov, *Surf. Sci.* **603**, L87 (2009).
- [23] <http://www.ioffe.ru/SVA/NSM/Semicond/SiC/thermal.html\#Lattice\%20properties>.
- [24] U. Starke in "Silicon Carbide: Recent Major Advances", Eds. W.J. Choyke, H. Matsunami and G. Pensl (Springer, 2004).
- [25] P. W. Tasker. *J. Phys. C: Solid State Phys.* **12**, 4977 (1979).
- [26] D. Vanderbilt, *Phys. Rev. B* **41**, 7892 (1990).
- [27] B. Hammer, O. H. Nielsen, J. J. Mortensen, L. Bengts-

- son, L.B. Hansen, A. C. E. Madsen, Y. Morikawa, T. Bligaard, A. Christensen, and J. Rossmeisl, available from <https://wiki.fysik.dtu.dk/dacapo>.
- [28] J. P. Perdew, K. Burke, and M. Ernzerhof, *Phys. Rev. Lett.* **77**, 3865 (1996).
 - [29] H. J. Monkhorst and J. D. Pack, *Phys. Rev. B* **13**, 5188 (1976).
 - [30] L. Bengtsson, *Phys. Rev. B* **59**, 12301 (1999).
 - [31] I. G. Batyrev, A. Alavi, and M. W. Finnis, *Phys. Rev. B* **62**, 4698 (2000)
 - [32] K. Reuter and M. Scheffler, *Phys. Rev. B* **65**, 035406 (2001).
 - [33] M. Dion, H. Rydberg, E. Schröder, D. C. Langreth, and B. I. Lundqvist, *Phys. Rev. Lett.* **92**, 246401 (2004).
 - [34] K. Lee, E. D. Murray, L. Kong, B. I. Lundqvist, and D. C. Langreth, *Phys. Rev. B* **82**, 081101(R) (2010).
 - [35] S.H. Vosko, L. Wilk, M. Nusair, *Can. J. Phys.* **58**, 1200 (1980).
 - [36] Y. Zhang and W. Yang, *Phys. Rev. Lett.* **80**, 890 (1998).
 - [37] E. D. Murray, K. Lee, and D. C. Langreth, *J. Chem. Theory Comput.* **5**, 2754 (2009).
 - [38] K Berland, T.L. Einstein, and P. Hyldgaard *Phys. Rev. B* **80**, 155431 (2009).
 - [39] S. D. Chakarova-Käck, E. Schröder, B. I. Lundqvist, and D. C. Langreth, *Phys. Rev. Lett.* **96**, 146107 (2006).
 - [40] K. Johnston, J. Kleis, B. I. Lundqvist, and R. M. Nieminen, *Phys. Rev. B* **77**, 121404(R) (2008).
 - [41] E. Ziambaras, J. Kleis, E. Schröder, and P. Hyldgaard, *Phys. Rev. B* **76**, 155425 (2007).
 - [42] E. Ziambaras, "Structure, bonding and transport of SiC and graphitic systems," PhD Thesis (Chalmers University of Technology, Göteborg, Sweden, 2006).
 - [43] J. Rohrer and P. Hyldgaard, *Phys. Rev. B* **82**, 045415 (2010); J. Rohrer and P. Hyldgaard, *J. Phys.: Condens. Matter* **22**, 472001 (2010).
 - [44] J. Rohrer, C. Ruberto, and P. Hyldgaard, *J. Phys.: Condens. Matter* **22**, 015004 (2010).
 - [45] F. C. Chuang, C. V. Ciobanu, V. B. Shenoy, C.Z. Wang, and K. M. Hoa, *Surf. Sci.* **573**, L375 (2004); M. Sierka, T. K. Todorova, J. Sauer, S. Kaya, D. Stacchiola, J. Weissenrieder, S. Shaikhutdinov, and H.-J.Freund, *J. Chem. Phys.* **126**, 234710 (2007).
 - [46] G. Kresse *et al.*, *Science* **308**, 1440 (2005).
 - [47] D. J. Wales and J. P. K. Doye, *J. Phys. Chem. A* **101**, 5111 (1997).
 - [48] S. Gödecke, *J. Chem. Phys.* **120**, 9911 (2004).

Relative stability of $6H$ -SiC{0001} surface terminations and formation of graphene overlayers by Si evaporation: Supplementary material

In the main article entitled 'Relative stability of $6H$ -SiC{0001} surface terminations and formation of graphene overlayers by Si evaporation', we investigate, among others, the relative stability of $6H$ -SiC{0001} surfaces as a function of their surface termination. Focusing on (1×1) surface unit-cells, we find that, independent of the orientation, Si termination is preferred over C termination. This result seems to be partially in conflict with intuition based on counting the number of dangling bonds; at SiC(000 $\bar{1}$), a C-terminated surface would be expected.

Here we present calculations where we consider the larger $(\sqrt{3} \times \sqrt{3})$ and (3×3) surface unit-cells. These cells, in principle, allow for various surface reconstructions, and the absence of such reconstructions in (1×1) surface unit-cells could be the origin of the counterintuitive prediction of a preferred Si termination at SiC(000 $\bar{1}$).

For all calculations we use a common 400 eV planewave cutoff. For $(\sqrt{3} \times \sqrt{3})$ surface cells, a $(3 \times 3 \times 1)$ k-point sampling is used; for (3×3) surface cells, a $(2 \times 2 \times 1)$ k-point sampling is used. The surfaces are modeled as slabs consisting of at least six SiC bilayers. All slabs are ideally truncated, that is, they possess either a full-coverage Si-terminated surface or a full-coverage C-terminated surface. The surface models are relaxed until the forces on atoms no longer exceeds 0.01 eV/Å.

Figure 7 details different (3×3) surface reconstructions obtained from our calculations. In fact, the direct relaxation of truncated surface slabs only produces flat surfaces without true reconstructions, the Si-terminated (3×3) (0001) surface being an exception. All other reconstructions are obtained by pulling one atom out of the flat surface-layer by 0.5 Å and then restarting the relaxations.

The most pronounced reconstruction, giving rise to triangular features, is identified at the C-terminated (3×3) (0001) surface, see set of mid-panels in Fig. 7. At Si-terminated (3×3) (0001), see set of top panels in Fig. 7, and Si-terminated (3×3) (000 $\bar{1}$), see set of bottom panels in Fig. 7, only smaller departures from the flat surface are found. The C-terminated (3×3) SiC(000 $\bar{1}$), remains unreconstructed even after triggering reconstructions by pulling atoms out of the surface.

For $(\sqrt{3} \times \sqrt{3})$ surface unit-cells, all but the Si-terminated (0001) configuration remain flat. The reconstruction of the Si-terminated $(\sqrt{3} \times \sqrt{3})$ (0001) surface is similar to the reconstruction of the Si-terminated (3×3) (0001) surface and therefore not shown.

The reconstructed configurations generally possess lower energies than their unreconstructed, flat counterparts. These energies are used in our comparison of surface energies in Table III in the paper.

We are aware of the likely fact that the here-presented reconstructions only represent a small sample of the rich

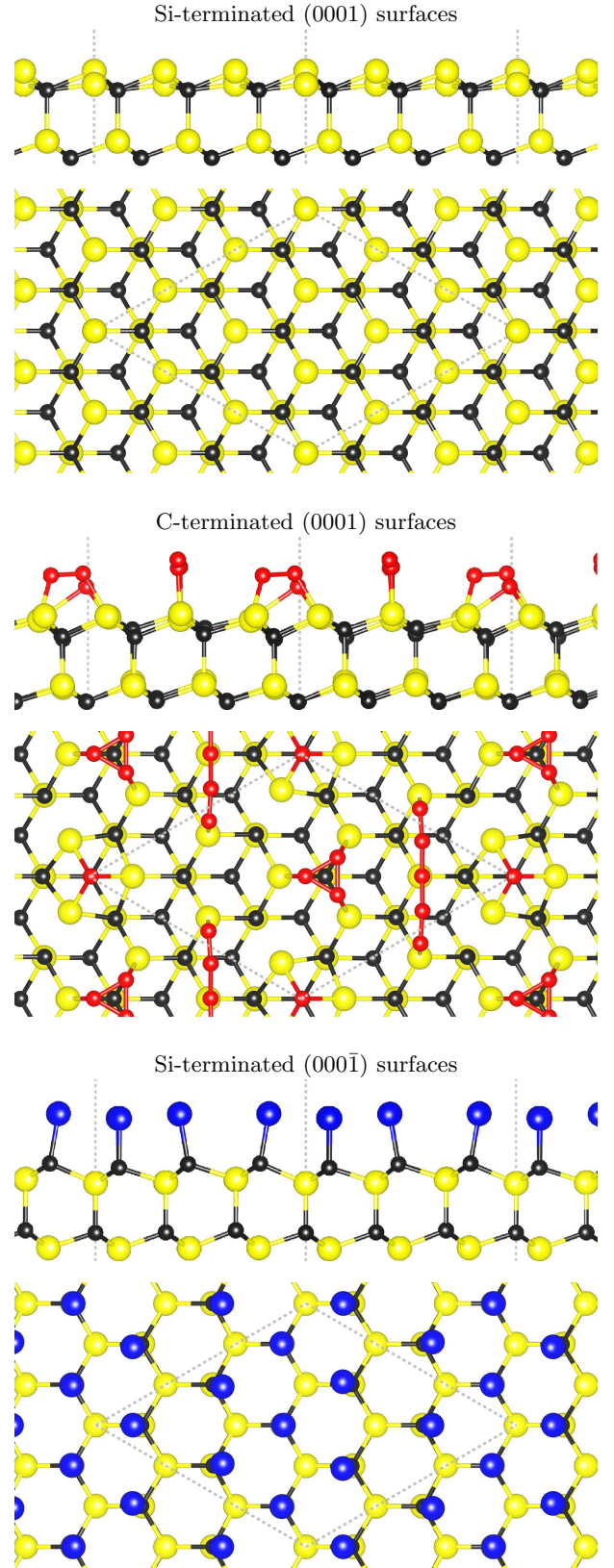


FIG. 7: Top and side views of (3×3) surface reconstructions identified in this study. Different colors are used to distinguish surface atoms that undergo strong rearrangements from those in subsurface layers.

SiC surface phase-diagram. The $(\sqrt{3} \times \sqrt{3})$ and (3×3) surface unit-cells allow for a large freedom in the variation of the coverage of surface Si or C. Closely related is the problem of identifying the lowest-energy structure for each coverage. A full reconstruction search would require more advanced strategies and methods than used here and is outside the scope of the present work.

Finally, we notice that identification of the full spec-

trum of surface reconstructions is in fact only of secondary relevance for the actual purpose of the main paper: the study of band-structure modifications due to van der Waals binding of graphitic overlayers at SiC{0001}. These overlayers arise from evaporation of Si atoms from SiC{0001}. As discussed in the main paper, the detailed structure and composition of the surface prior to evaporation may be only of minor relevance.